Single and multi-layered core-shell structures based on ZnO nanorods obtained by aerosol assisted chemical vapor deposition

A. Sáenz-Trevizo, P. Amézaga-Madrid, P. Pizá-Ruiz, W. Antúnez-Flores, C. Ornelas-Gutiérrez, M. Miki-Yoshida

Abstract

Core–shell nanorod structures were prepared by a sequential synthesis using an aerosol assisted chemical vapor deposition technique. Several samples consisting of ZnO nanorods were initially grown over TiO2 film-coated borosilicate glass substrates, following the synthesis conditions reported elsewhere. Later on, a uniform layer consisting of individual Al, Ni, Ti or Fe oxides was grown onto ZnO nanorod samples forming the so-called single MO_x/ZnO nanorod core–shell structures, where MO_x was the metal oxide shell. Additionally, a three-layer core–shell sample was developed by growing Fe, Ti and Fe oxides alternately, onto the ZnO nanorods. The microstructure of the core–shell materials was characterized by grazing incidence X-ray diffraction, scanning and transmission electron microscopy. Energy dispersive X-ray spectroscopy was employed to corroborate the formation of different metal oxides. X-ray diffraction outcomes for single core–shell structures showed solely the presence of ZnO as wurtzite and TiO2 as anatase. For the multi-layered shell sample, the existence of Fe2O3 as hematite was also detected. Morphological observations suggested the existence of an outer material grown onto the nanorods and further microstructural analysis by HR-STEM confirmed the development of core–shell structures in all cases.

These studies also showed that the individual Al, Fe, Ni and Ti oxide layers are amorphous; an observation that matched with X-ray diffraction analysis where no apparent extra oxides were detected. For the multilayered sample, the development of a shell consisting of three different oxide layers onto the nanorods was found. Overall results showed that no alteration in the primary ZnO core was produced during the growth of the shells, indicating that the deposition technique used herein was and it is suitable for the synthesis of homogeneous and complex nanomaterials high in quality and purity. In addition, materials absorptance determined from the total transmittance and reflectance spectra revealed a broader absorption interval including visible light, indicating potential uses of these nanostructures on solar energy appliances.

Introduction

One-dimensional structures in the form of nanorods and nanowires are desired morphologies for many applications, due to their geometrical configuration, which provides a higher surface-to-volume ratio [1–11]. As a consequence, these materials can be used as more effective photocatalysts [3, 10–15], UV photodetectors [16], and in different optoelectronic [1, 2, 9, 17], photovoltaic [18–22], or electrochemical devices [23–25]. Core–shell structures have attracted considerable attention for previous applications since the surface properties of the core material, such as its chemical stability, electrical and optical properties, can be enhanced or modified by creating a proper combination of materials [1–3, 12, 13, 15–17, 22–24]. ZnO is a promising candidate for core–shell structure fabrication because of its well-known chemical and physical properties, apart from its low cost and easy fabrication by different techniques

[4–6, 11–17,19–24]. In fact, it has already been coupled with various binary and ternary compounds, including CdS [1,14], Al2O3 [2], CuO [3], NiO [7,17], Bi2O3 [11], Fe2O3 [15], HfO2 [16], Cu2O [22], TiO2 [13, 19–21,23], SrTiO3 [12], Zn2SnO4 [24] and ZnS [25] in order to search for more efficient and durable materials, that are commonly applied as solar cells, photocatalysts for water treatment or H2 production, batteries, sensors, among others. Through the combination of ZnO with metal oxides, its chemical stability and optical response are improved [3, 15, 19, 20, 23]. Low temperature synthesis processes, such as hydrothermal ones, are sometimes the preferred methods for the preparation of ZnO nanorod based core–shell structures [2, 9, 23]. Nevertheless, these methods require an additional annealing stage, increasing time and energy consumption. Alternative processes for core–shell structure synthesis come through the combination of different consecutive techniques [1–3,7,11,14–17,19–24], a procedure that implies longer synthesis periods and the use of more equipment, reactants and materials, deriving in a time consuming and expensive process. Besides, and particularly within the employment of ZnO as a core, the selection of the shell synthesis method has to consider the chemical characteristics of the precursors (based on the pH), in order to prevent the core dissolution, as stated previously by different authors [11, 17, 19–25]. In contrast, the aerosol assisted chemical vapor deposition method (AACVD) can advantageously synthesize many types of nanostructured materials, including core–shell structures, employing the same equipment [26–28].

In compliance with previous information, this work focuses on the synthesis of core–shell structures based on ZnO nanorods (core) and uniform layers (single and multi) of other oxides (shell), deposited by an aerosol assisted CVD technique

performed in a sequential mode. Shell materials were chosen to improve optical absorption in the visible interval and to protect the ZnO nanorod for potential applications. Afterwards, a complete microstructural characterization of the core–shell structures by grazing incidence X-ray diffraction (GIXRD) as well as electron microscopy was presented. Additionally, the optical absorptance determination of the nanostructures was also performed.

Materials and methods

-Samples synthesis

All ZnO nanorod samples used as core structures were grown onto TiO2 coated borosilicate glass substrates using the AACVD technique. The synthesis followed the general configuration, with starting solutions and conditions reported previously in [26]. A bare ZnO nanorod sample, used as reference, was labeled as Z structure. The Al, Fe, Ti and Ni individual precursor solutions for the synthesis of the shells were prepared in methanol (99.8%), at concentrations of 0.075, 0.1, 0.05 and 0.1 mol.dm−3, respectively. Aluminum acetylacetonate (99%), iron acetylacetonate (99%), titanium (IV) oxyacetylacetonate (90%), and nickel (II) acetate tetrahydrate (98%) were used as precursor salts. Deposition temperature for all shell layers was 673 K. Oil-free and filtered air was used as the carrier gas and was fed into a mass flow- controller at a constant pressure of 2.8 × 105 Pa. The controller supplied the carrier air at a constant flow directly into the nebulization chamber, which was loaded with the precursor solution. Nebulization of the solution was carried out with an ultrasonic nebulizer (Sonaer-241) operated at 2.4 MHz. The precursor aerosol of the different sources was injected separately onto the bare ZnO nanorod samples in order to obtain the

corresponding shell layer. Injection of the aerosol was accomplished by a movable nozzle, which uniformly coated the entire surface. The scan velocity of the nozzle was selected according to each layer. The most important synthesis conditions and the adopted nomenclature for the obtained samples appear summarized in Table 1.

Table 1
Principal parameters used for the growth of the different shell material.

Sample	Shell material	Air flux [$dm^3 \cdot s^{-1}$]	Nozzle scan velocity [$cm \cdot s^{-1}$]
A	AlO_x	5.8×10^{-2}	3.3×10^{-3}
N	NiO	8.3×10^{-2}	6.6×10^{-3}
T	TiO_x	1.7×10^{-1}	6.6×10^{-3}
F	FeO_x	8.3×10^{-2}	10^{-2}
FTF	$FeO_x/TiO_2/FeO_x$	$8.3 \times 10^{-2}/1.7 \times 10^{-1}/8.3 \times 10^{-2}$	$10^{-2}/6.6 \times 10^{-3}/10^{-2}$

-Characterization

Grazing incidence X-ray diffraction patterns were measured in order to determine the crystalline phases on the synthesized samples. The measurements were carried out in a PANalytical X'Pert system, employing the following conditions: a Cu Kα radiation (λ = 0.1542 nm) operated at 40 keV and 30 mA, a grazing angle of 0.5°, a scanning angle 2θ varied in a range from 20° to 80°, with a step size of 0.05° and 2.75 s of step time. Surface morphology was analyzed by scanning electron microscopy (SEM) in a field emission JEOL JSM-7401F microscope. Microstructure determination of the samples was accomplished by high resolution scanning transmission electron microscopy (HR-STEM) in a JEOL JEM- 2200FS + Cs equipped with a probe spherical aberration corrector and operated at an accelerating voltage of 200 kV. For HR-STEM observations, nanorods were scratched from each sample and placed directly onto holey-carbon coated TEM grids. Energy dispersive X-ray spectroscopy (EDXS) in linescan mode was performed with an Oxford Inca X-sight detector attached to the

TEM. The absorptance spectrum of the materials was determined from the total reflectance and transmittance measurements in the UV–VIS–NIR interval in a CARY 5000 spectrophotometer with a DRA2500 integrating sphere accessory.

Results and discussion

-Crystalline structure, morphology and composition

Diffraction patterns obtained by GIXRD are shown in Fig. 1, where it is clear that in all cases, samples exhibited the crystalline character of ZnO (wurtzite) and TiO2 (anatase) phases. Both components were related with the existence of the ZnO nanorods and the TiO2 buffer film de- posited onto the borosilicate substrates (sample Z) as previously presented [26]. The identified phases matched with JCPDF cards 01- 073-8765 [29] and 00-021-1272 [30], respectively. For samples A, F and N, no precise diffracting lines corresponding to the oxides of these elements (Al, Fe and Ni) were detected. In contrast, GIXRD pattern for sample FTF (Fig. 1(b)) revealed the formation of two additional small peaks at about 24.2 and 33.3°, which indicated the presence of iron oxide (Fe2O3) as hematite. Previous identification was in accordance with the diffraction file JCPDF 01-084-0308 [31] for this material. Results from the depicted analysis were confirmed by HR-STEM analysis as described below.

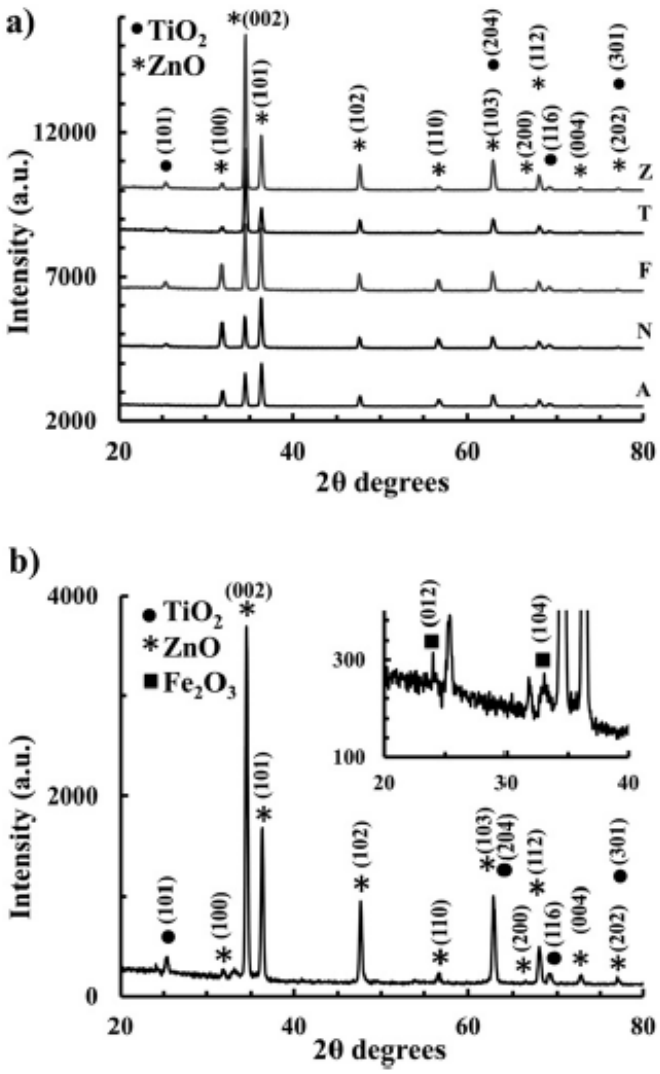

Fig. 1. GIXRD patterns of the ZnO nanorod (core)–oxide layer (shell) nanostructures synthesized by the AACVD technique. a) For bare ZnO nanorod (Z), Ti (T), Fe (F), Ni (N) and Al (A) core–shell structures; b) multi-layered shell sample FeO_x–TiO_2–Fe_2O_3 (FTF). All structures exhibited the presence of TiO_2 (anatase) and ZnO (wurtzite) phases, which were the Z material components.

According to SEM observations, all samples exhibited the typical polygonal prism morphology of ZnO nanorods obtained by the current AACVD technique as reported previously [26]. Samples showed well-distributed nanorods deposited onto the surface of the substrates. Nanorods on sample Z presented well-defined prisms with a hexagonal cross-section and planar facets with sharp edges, as seen in Fig. 2(a). This

geometrical configuration matched with information presented in Ref. [26]. Average nanorod length and width (distance between op- posed facets) was determined as 1.5 ± 0.2 μm and 350 ± 180 nm, respectively. Size information was obtained from SEM cross-section and top view micrographs. For sample A, in Fig. 2(b), slight evidence of an additional layer was perceptible, as the edges of the columnar bodies appeared rounded, contrary to those sharp edges seen on sample Z. In the case of sample N in Fig. 2(c), similar structures as those in sample A were seen, but numerous tiny granular elongated particles distributed onto the faces of the columns were visible, indicating the formation of an extra layer of material onto the nanorods. A detailed observation of Fig. 2(d) from sample F shows many small grains on the columns, which modified the smooth and flat aspect of the bare ZnO nanorod facets. Sample T, whose SEM micrograph was obtained at high magnifications, appears in Fig. 2(e). The micrograph shows the presence of a granular material covering the surface of the nanorods. Otherwise, SEM micrograph of sample FTF in Fig. 2(f) displays an obvious alteration and the original sharp definition of the nanorod surface. For this sample, the external coating presented a clear granular formation that covered the entire surface uniformly and so, the development of a shell material was suggested. As no additional crystalline phases were detected for samples A, N, F and T by GIXRD analysis, morphological changes on the ZnO nanorods were taken as indication of the core–shell structure development.

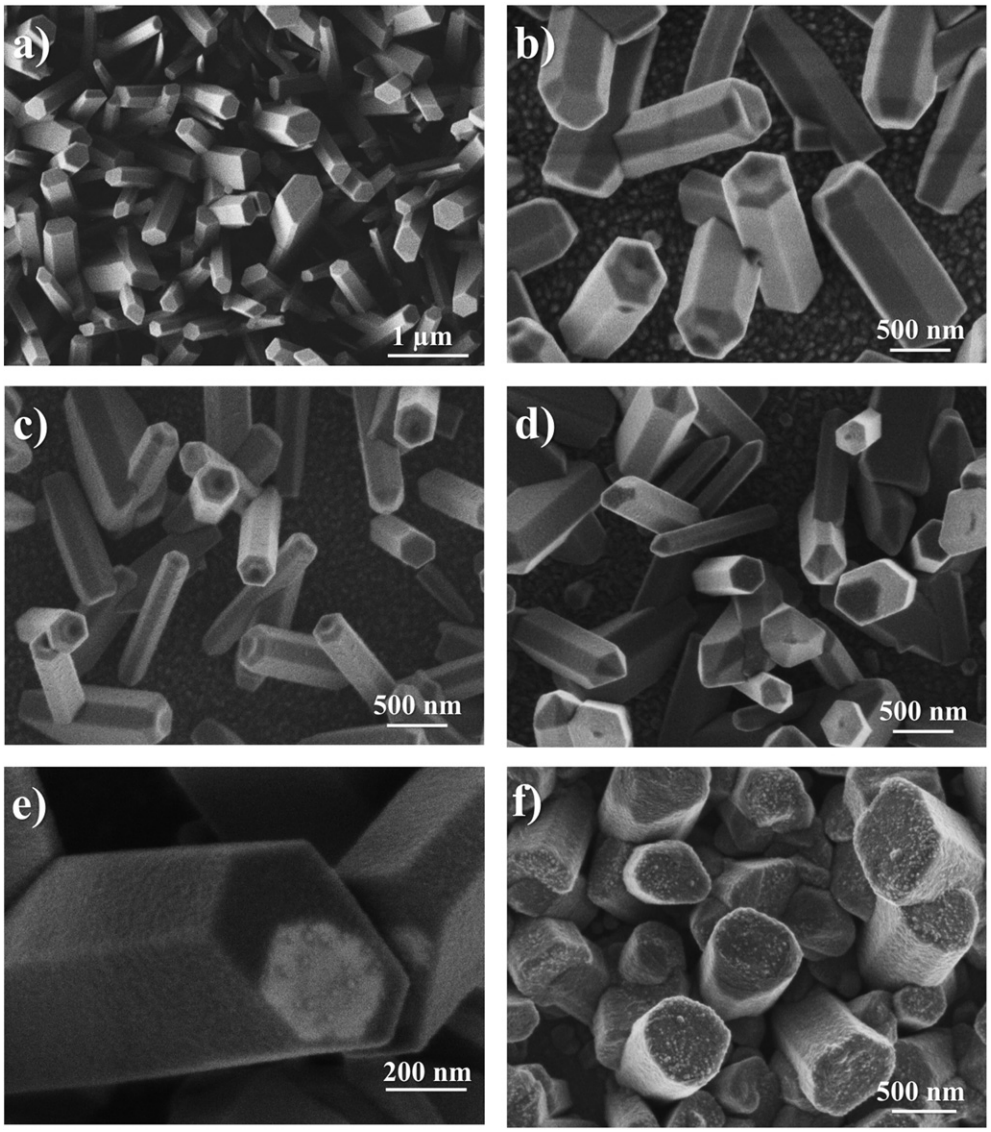

Fig. 2. Secondary electron SEM micrographs showing the surface modifications of ZnO nanorods (core) covered with different oxide layers (shell): a) bare ZnO (Z); b) AlO_x (A); c) NiO (N);
d) FeO_x (F); e) TiO_x (T) and f) $FeO_x/TiO_2/Fe_2O_3$ (FTF).

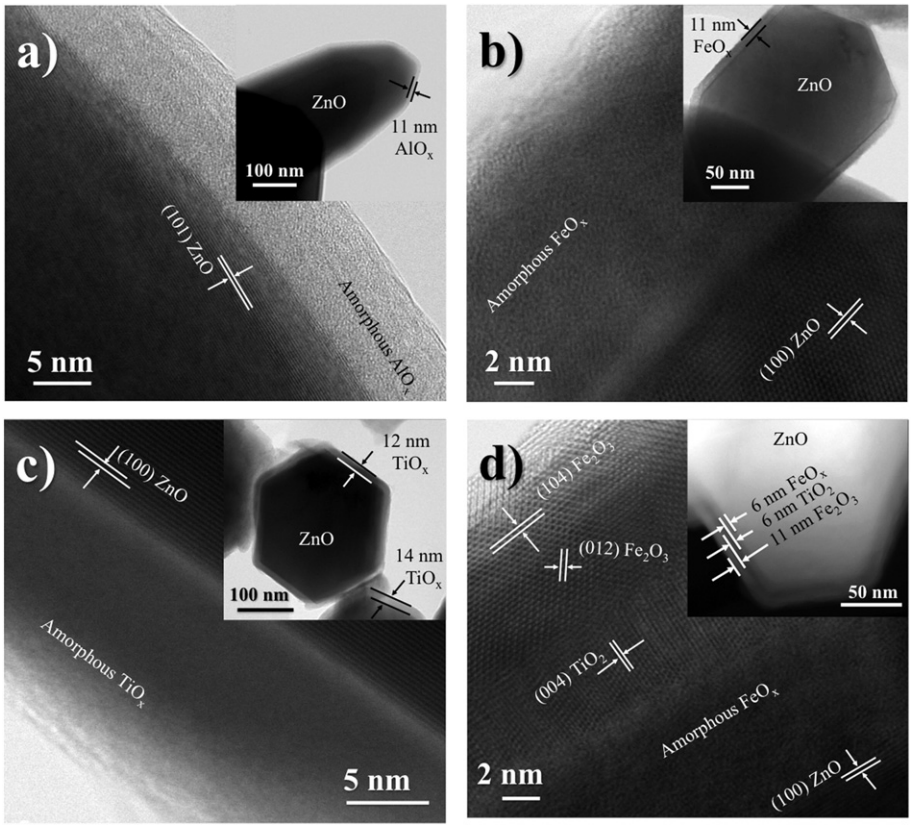

Fig. 3. Bright field STEM micrographs showing the core–shell structure of samples: a) A, b) F, c) T and d) FTF. Crystalline ZnO nanorod core was detected in all cases. Insets display the uniform distribution and thickness of the single and multi-layered shell around the ZnO core.

Additional microstructural analysis of individual nanorods from each sample was performed by HR-STEM. Results are shown in bright field STEM micrographs of Fig. 3. As depicted previously in [26], all of the observed ZnO nanorods were monocrystalline and exhibited their longitudinal axis along the [001] direction, a crystalline arrangement that has been grown irrespective from the precursors employed [5] and which is the preferred orientation reported for the wurtzite structure obtained by various synthesis methods [2–6,8,10,11,14,16,18,22, 23,25,27]. For sample A in Fig. 3(a), a core–shell structure was noticed as a clear difference in contrast caused by the presence of different components, ZnO and AlO_x. Also, the crystalline structure of ZnO nanorods was identified by measurements of lattice fringes from this micrograph. Furthermore, the

shell layer was observed as a uniform amorphous coating of AlO_x deposited onto the nanorods. Its average thickness was determined as 9 ± 1 nm. Fig. 3(b) shows a micrograph from sample F, which also exhibited the formation of a ZnO nanorod core–FeO_x shell structure. The shell layer was amorphous, uniform and well- distributed over the entire nanorod surface. Its thickness was deter- mined as 11 ± 1 nm. Fig. 3(c) shows the morphology of sample T. The TiO_x layer was again amorphous, uniform and continuous, having a thickness of about 14 ± 3 nm. Because of the amorphous aspect of the shell in samples A, F and T, the identification of oxides from the different sources was not possible from the earlier discussed X-ray diffraction analysis. For sample FTF in Fig. 3(d) a uniform shell comprising three different materials was observed in the ZnO nanorods. The formation of the ZnO nanorod core was recognized within lattice fringes in this figure. The total thickness of the resulting shell was determined as 25 ± 3 nm. The multi-layered shell sample revealed clear lattice fringes, in contrast to the single layer shell materials. However, the first shell of Fe oxide (adjacent to the nanorod) was amorphous, and the second and third corresponding to the Ti and Fe oxide layers, respectively, were crystalline. Measured lattice fringes from the second and third shells matched with crystallographic information of anatase TiO2 and hematite Fe2O3 phases, respectively, also in agreement with GIXRD results in Fig. 1(b). Additional low magnification STEM micrograph, taken from samples A, F, T and FTF appear as insets in Fig. 3. All of the insets show the homogeneity of the depicted core–shell structures obtained by the current synthesis method. The thickness of the shell layers was measured and marked for all samples in order to display the uniform distribution of the

coatings. From the Z-contrast micrograph of sample FTF shown as inset in Fig. 3(d), it was possible to clearly discern the three different components of the shell coating.

Further EDXS analyses were accomplished in linescan mode in order to corroborate the formation of different metal oxides in the core–shell structure. A quantitative linescan microanalysis was performed to sample A. Results appear in Fig. 4, which also displays the image of the linescan zone in (a). It is clear from Fig. 4(b), that the distribution of Al, Zn and O indicate the formation of an Al oxide shell around the ZnO nanorod, confirming the development of a core–shell structure. Additional qualitative EDXS linescan profiles of sample T appear in Fig. 5(a) and (b). From Fig. 5(b), a clear distribution of the constituent elements Zn, Ti and O shows that there is a Ti oxide shell layer covering the ZnO nanorod core. Fig. 6(a) and (b) shows the qualitative linescan microanalysis of sample FTF. As in previous samples, the distribution of Zn, Fe, Ti and O evidenced the establishment of three different shell layers, i.e. $FeO_x/TiO_x/FeO_x$ enveloping the ZnO nanorod core.

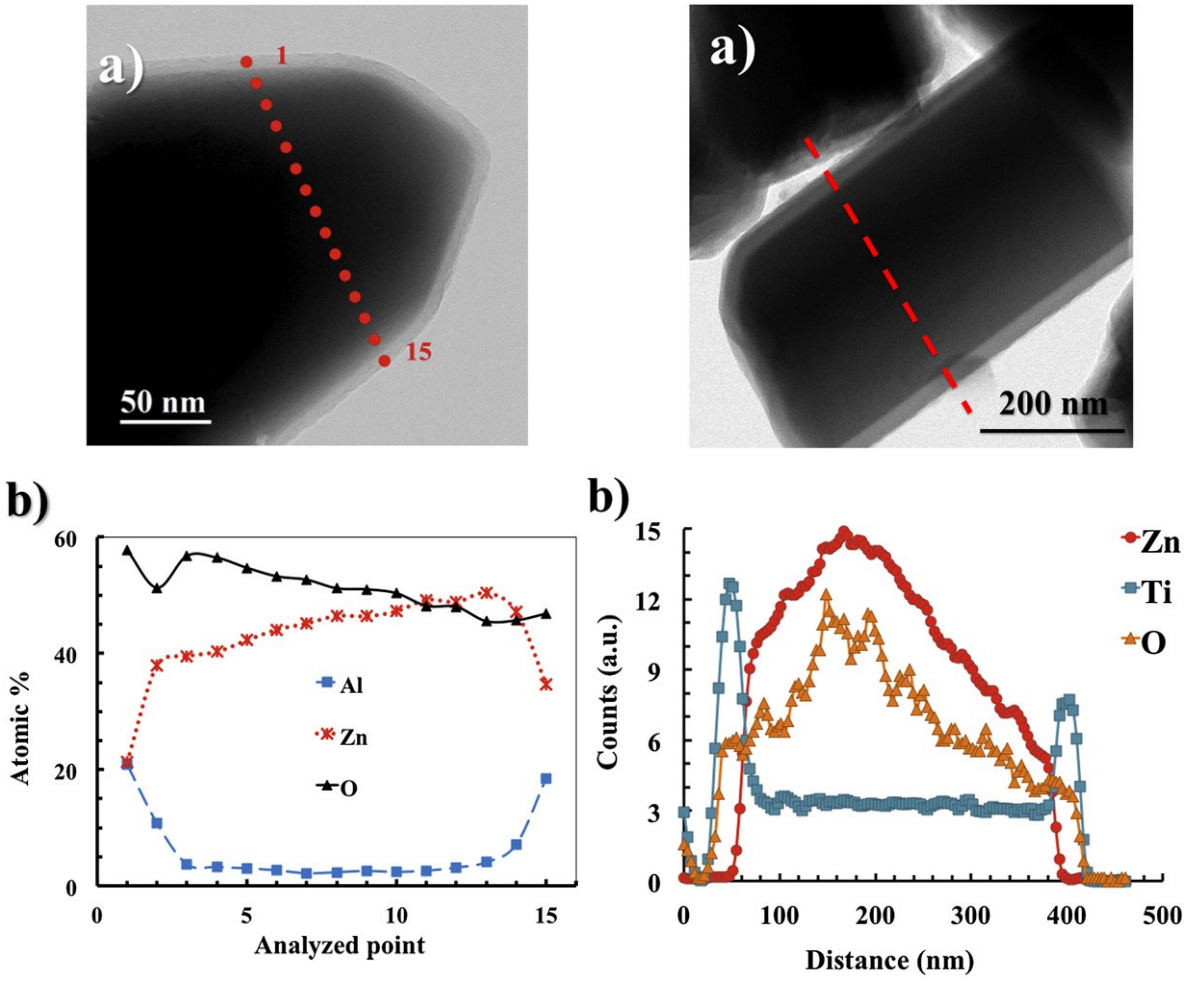

Fig. 4. a) Bright field STEM micrograph of sample A, showing the area of the quantitative EDXS linescan (dotted line). b) Al, Zn and O composition in at.%, for each point along the dotted line shown in a).

Fig. 5. Results of qualitative EDXS linescan of sample T. a) STEM micrograph of the ana- lyzed line (dashed line); b) Zn distribution (●), Ti distribution (■) and O distribution (▲). Element distributions corroborate the formation of a non-mixed metal oxide shell.

Overall outcomes obtained so far indicate that no corrosion effects, dissolution, mixture of materials or defective formations on the ZnO nanorod core were produced during the shell growth. This information validates the AACVD technique employed herein as suitable for the synthesis of core–shell structures in a sequential step, including multilayered shell samples. Results were in opposition to the reports of Wang

[11] and Liu [15] who observed the development of nanotube structures after the deposition of the shell. The later as the precursors consumed the core material, confirming that ZnO dissolves in aqueous and acidic media [11, 12, 15–17,19–21,25]. As a consequence, to avoid core dissolution, the use and combination of different methods for the core and shell formation was required, taking into account that the acidic or basic nature of the precursor will not affect the integrity of the primary ZnO structure. In fact, a multilayered core–shell structure was already presented by Krunks et al. [19]. However, the multiple layers were mainly incorporated to protect ZnO from dissolution. Favorably, for all the cases presented herein, the columnar structure of the nanorods was preserved and no material was washed away during the shell deposition. On the other hand, Huang et al. [25] previously reported another successful two-step method for the synthesis of core–shell structures using solely the thermal evaporation technique. Nevertheless, the simplicity of the AACVD method and equipment employed in this work represents a convenient option for incorporation in large-scale applications.

-Optical properties

Absorption behavior of materials was analyzed in the region from 300 to 2500 nm, which corresponds to energy values from about 4.1 to 0.5 eV. Due to the rough surface of ZnO nanostructures, diffuse scattering must be considered. Then, absorptance (A) of the material can be defined as follows [32]:

AðλÞ ¼ 1−TðλÞ−RðλÞ−SðλÞ

where T(λ) is the direct transmittance, R(λ) is the specular reflectance and S(λ) is the diffuse scattering. Considering total transmittance (Tt) and total reflectance (Rt), i.e.

taking into account specular and diffuse components, the diffuse scattering term S is included in these quantities; consequently absorptance can be expressed as:

$Aðλ Þ ¼ 1 - T_t ðλ Þ - R_t ðλ Þ$:

Absorptance spectra as a function of photon energy, was calculated from total reflectance and total transmittance measurements. Results are shown in Fig. 7. From the figure it is seen that samples exhibited the absorption edge related to interband transition in ZnO nanorods at around 3.2 eV, as reported elsewhere [7,8]. However, for some nanostructures remarkable differences were noticed in the visible region. Samples with Fe oxide shell showed from 60 to 75% of absorptance in the visible region; extending the absorption interval, from UV region up to 2.2 eV, which implies that, a considerable part of the visible light was absorbed by the shell material. This behavior was seen in samples F and FTF, which in fact presented the highest absorption in both UV and VIS regions, in comparison with the samples. The observed light absorption behavior of these samples can be attributed to the presence of the FeO_x layer. Samples A, N and T showed no significant differences in their optical properties when compared to Z sample. The expected modification of absorptance due to the combination of oxides was confirmed and results were very similar to those in some references [12, 15, 18–20, 23–25].

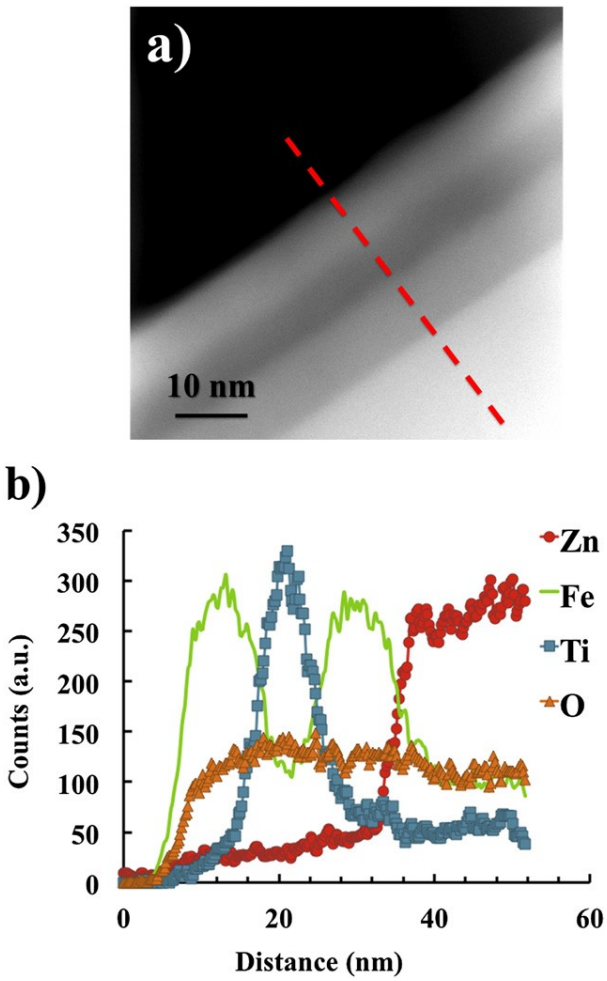

Fig. 6. Results of qualitative EDXS linescan of sample FTF. a) Z contrast micrograph of the analyzed core–shell structure (dashed line); b) Zn distribution (●), Fe distribution (–), Ti distribution (■) and O distribution (▲). Element distributions confirmed the formation of non-mixed $FeO_x/TiO_2/Fe_2O_3$ shells.

Conclusions

A series of single ZnO nanorod (core)–metal oxide (shell) and ZnO nanorod (core)–multilayered metal oxide (shell) samples were successfully fabricated using only the AACVD technique in a sequential process. Samples were structurally uniform and no defects were noticed. For all samples, the first shell was amorphous; however, when second and third shell layers were grown, the development of crystalline phases resulted. Average width and length of ZnO nanorod core were of 350 ± 180 nm and 1.5

± 0.2 μm, respectively. Individual shell thick- ness was around 10 nm. Additionally, broader light absorption observed on the samples caused by the coupling of different metal oxides could be suitable for optical and photochemical applications. Results demonstrated that the AACVD method alone could be implemented advantageously for the sequential formation of multi-layered core–shell materials, reducing synthesis time and avoiding the application of unnecessary materials and equipment.

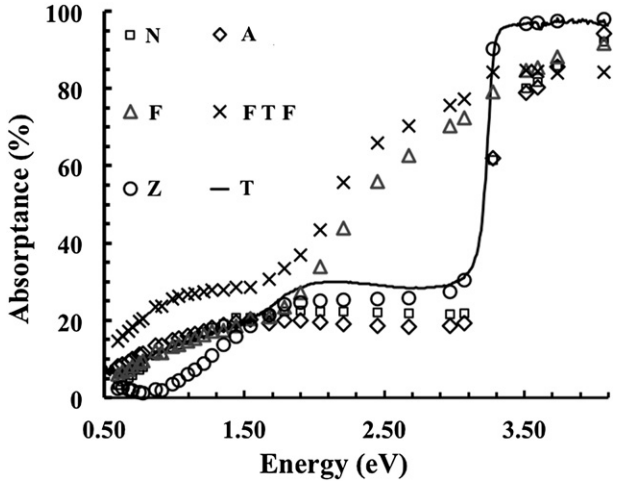

Fig. 7. Optical absorptance of the core–shell nanostructures as a function of photon energy. The incorporation of Fe oxide resulted in a broader light absorption, extending to visible interval.

Acknowledgments

The authors would like to thank to the following people: E. Torres, S. Miranda, O. Solis, C. Leyva, K. Campos, E. Guerrero, O. Esquivel and M. Lugo for the technical assistance they provided during the execution of this work. They would also like to thank SEP-CONACYT (project no. 242612) for their partial financial support.

References

[1] Q. Yang, Y. Li, Z. Hu, Z. Duan, P. Liang, J. Sun, N. Xu, J. Wu, Extended photo-response of ZnO/CdS core/shell nanorods fabricated by hydrothermal reaction and pulsed laser deposition, Opt. Express 7 (22) (2014) 8617–8623.

[2] C.Y. Chen, C.A. Lin, M.J. Chen, G.R. Lin, J.H. He, ZnO/Al2O3 core–shell nanorod arrays: growth, structural characterization, and luminescent properties, Nanotechnology 20 (18) (2009) 185605–185610.

[3] Q. Simon, D. Barreca, A. Gasparotto, C. Maccato, T. Montini, V. Gombac, P. Fornasiero,
O.I. Lebedev, S. Turner, G.V. Tendeloo, Vertically oriented CuO/ZnO nanorod arrays: from plasma-assisted synthesis to photocatalytic H2 production, J. Mater. Chem. 22 (2012) 11739–11747.

[4] D. Barreca, D. Bekermann, A. Devi, R.A. Fischer, A. Gasparotto, C. Maccato, E. Tondello, M. Rossi, S. Orlanducci, M.L. Terranova, Novel insight into the alignment and structural ordering of supported ZnO nanorods, Chem. Phys. Lett. 500 (2010) 287–290.

[5] D. Bekermann, A. Ludwig, T. Toader, C. Maccato, D. Barreca, A. Gasparotto, C. Bock,
A.D. Wieck, U. Kunze, E. Tondello, R.A. Fischer, A. Devi, MOCVD of ZnO films from bis(ketoiminato)Zn(II) precursors: structure, morphology and optical properties, Chem. Vap. Depos. 17 (2011) 155–161.

[6] D. Bekermann, A. Gasparotto, D. Barreca, L. Bovo, A. Devi, R.A. Fischer, O.I. Lebedev, C. Maccato, E. Tondello, G.V. Tendeloo, Highly oriented ZnO nanorod arrays by a novel plasma chemical vapor deposition process, Cryst. Growth Des. 10 (2010) 2011–2018.

[7] R.-C. Wang, M.-G. Chen, Enhanced photosensing and tunable luminescence from ZnO/NiO and ZnO/Ni core–shell nanorods, Sensors Actuator B 178 (2013) 212–216.

[8] K.L. Foo, U. Hashim, K. Muhammad, C.H. Voon, Sol–gel synthesized zinc oxide nano- rods and their structural and optical investigation for optoelectronic application, Nanoscale Res. Lett. 429 (2009) 1–10.

[9] M. Krunks, T. Dedova, Karber, V. Mikli, I. Oja Acik, M. Grossberg, A. Mere, Growth and electrical properties of ZnO nanorod arrays prepared by chemical spray pyroly- sis, Physica B 409 (2009) 4422–4425.

[10] X. Li, J. Wang, J. Yang, J. Lang, S. Lü, M. Wei, X. Meng, C. Kou, X. Li, Comparison of pho- tocatalytic activity of ZnO rod arrays with various diameter sizes and orientation, J. Alloys Compd. 580 (2013) 205–210.

[11] Z.-L. Wang, R. Guo, G.-R. Li, L.-X. Ding, Y.-N. Ou, Y.-X. Tong, Controllable synthesis of ZnO-based core/shell nanorods and core/shell nanotubes, RSC Adv. 1 (2011) 48–51.

[12] Y.F. Tu, Q.M. Fu, X.J. Niu, J.P. Sang, Z.J. Tan, G. Zheng, X.W. Zou, Fabrication and pho- tocatalytic property of ZnO/SrTiO3 core/shell nanorod arrays, J. Cryst. Res. Technol. 48 (3) (2013) 138–144.

[13] R. Wang, H. Tan, Z. Zhao, G. Zhang, L. Song, W. Dong, Z. Sun, Stable ZnO@TiO2 core/ shell nanorod arrays with exposed high energy facets for self-cleaning coatings with anti-reflective properties, J. Mater. Chem. A 2 (2014) 7313–7318.

[14] S. Khanchandani, S. Kundu, A. Patra, A.K. Ganguli, Shell thickness dependent photo- catalytic properties of ZnO/CdS core–shell nanorods, J. Phys. Chem. C 116 (2012) 23653–23662.

[15] Y. Liu, L. Sun, J. Wu, T. Fang, R. Cai, A. Wei, Preparation and photocatalytic activity of ZnO/Fe2O3 nanotube composites, Mater. Sci. Eng. B 194 (2015) 9–13.

[16] X. Zhang, L. Zhang, G. Yan, J. Shen, M. Gao, J. Li, H. Dong, D. Zhao, L. Cai, Q. Chen, W. Zhou, S. Xie, Optical and electrical performance of HfO2 coated ZnO nanorod arrays,
J. Nanosci. Nanotechnol. 13 (2013) 1082–1086.

[17] M.-S. Wu, H.-W. Chang, Self-assembly of NiO-coated ZnO nanorod electrodes with core–shell nanostructures as anode materials for rechargeable lithium-ion batteries, J. Phys. Chem. C 117 (2013) 2590–2599.

[18] C.Y. Dwivedi, V. Dutta, Vertically aligned ZnO nanorods via self-assembled spray py- rolyzed nanoparticles for dye-sensitized solar cells, Adv. Nat. Sci.: Nanosci. Nanotechnol. 3 (2012) 015011–015019.

[19] M. Krunks, A. Katerski, T. Dedova, Acik I. Oja, A. Mere, Nanostructured solar cell based on spray pyrolysis deposited ZnO nanorod array, Sol. Energy Mater. Sol. Cells 1016–1019 (2008).

[20] L.E. Greene, M. Law, B.D. Yuhas, P. Yang, ZnO–TiO2 core–shell nanorod/P3HT solar cells, J. Phys. Chem. C 111 (2007) 18451–18456.

[21] Acik I. Oja, A. Katerski, A. Mere, J. Aarik, A. Aidla, T. Dedova, M. Krunks, Nanostruc- tured solar cell by spray pyrolysis: effect of titania barrier layer on the cell performance, Thin Solid Films 517 (2009) 2443–2447.

[22] Y.-S. Chen, C.-H. Liao, Y.-L. Chueh, C.-C. Lai, L.-Y. Chen, A.-K. Chu, C.-T. Kuo, H.-C. Wang, High performance Cu2O/ZnO core–shell nanorod arrays synthesized using a nanoimprint GaN template by the hydrothermal growth technique, Opt. Mater. Express 4 (7) (2014) 1475–1486.

[23] S. Panigrahi, D. Basak, Core–shell TiO2@ZnO nanorods for efficient ultraviolet photodetection, Nanoscale 3 (2011) 2336–2341.

[24] T. Bora, H.H. Hyaw, J. Dutta, Zinc oxide–zinc stannate core–shell nanorod arrays for CdS quantum dot sensitized solar cells, Electrochim. Acta 68 (2012) 141–145.

[25] X. Huang, M. Wang, M.-C. Willinger, L. Shao, D.-S. Su, X.M. Meng, Assembly of three- dimensional hetero-epitaxial ZnO/ZnS core/shell nanorod and single crystalline hol- low ZnS nanotube arrays, ACS Nano 6 (8) (2012) 7333–7339.

[26] A. Sáenz-Trevizo, P. Amézaga-Madrid, L. Fuentes-Cobas, P. Pizá-Ruiz, W. Antúnez- Flores, C. Ornelas-Gutiérrez, S.A. Pérez-García, M. Miki-Yoshida, Microstructural, chemical and textural characterization of ZnO nanorods synthesized by aerosol assisted chemical vapor deposition, Mater. Charact. 98 (2014) 215–221.

[27] A. Sáenz-Trevizo, P. Amézaga-Madrid, P. Pizá-Ruíz, O. Solís-Canto, C. Ornelas-Gutiérez, S. Pérez-García, M. Miki-Yoshida, Microstructural characterization, optical and photocatalytic properties of bilayered CuO and ZnO based thin films, J. Alloys Compd. 615 (1) (2014) S375–S381.

[28] P. Amézaga-Madrid, A. Hurtado-Macías, W. Antúnez-Flores, F. Estrada-Ortíz, P. Pizá- Ruiz, M. Miki-Yoshida, Synthesis, microstructural, optical and mechanical properties of yttria stabilized zirconia thin films, J. Alloys Compd. 536S (2012) S412–S417.

[29] ICDD XRD database PDF number 01-075-1533 (1997).

[30] ICDD XRD database PDF number 00-021-1272 (1990).

[31] ICDD XRD database PDF number 01-084-0308 (1980).

[32] O. Stenzel, The Physics of Thin Films Optical Spectra, Springer-Verlag, Berlin, 2005. 73 (Chapter 6).